An Investigation on The Effects of Various Flow Parameters on the Underwater Flow Noise

SERTAC BULUT[a] and SELMA ERGİN[b]

[a] *Istanbul Technical University, Faculty of Naval Architecture and Ocean Engineering, Maslak 34469, Istanbul, Turkey.*

[b] *Istanbul Technical University, Faculty of Naval Architecture and Ocean Engineering, Maslak 34469, Istanbul, Turkey.*

Abstract. The prediction and reduction of underwater noise is commercially, militarily and ecologically a very critical issue for maritime industry. Machine noise, propeller noise and flow noise are the main components of underwater noise for submerged bodies. Especially at high flow velocities, flow noise becomes dominant source of underwater noise radiated from these bodies. In this paper, the effects of the fluid temperature and salinity of the fluid on the underwater flow noise are investigated, numerically. A circular cylinder is selected for the validation studies of the noise model used in the acoustic analyses. The flow characteristics are obtained by solving governing equations of fluid using Computational Fluid Dynamics (CFD). The turbulence is modelled by using SST k-ω turbulence model. The Ffowcs Williams and Hawkings (FW-H) noise model is applied to predict the sound pressure levels at the receiver points defined various locations, numerically. The monopole, dipole and quadrupole sound sources are taken into consideration for acoustic analyses.

Keywords. Underwater Flow Noise, Computational Acoustics, FW-H, sound sources.

1. Introduction

Underwater flow-induced noise has become an important issue today because of adverse effects of the current levels of noise produced by submerged bodies and vessels on aquatic life. Understanding of the impacts of underwater noise on marine organisms depends on knowledge of its feature. In the sea, variations in the properties of seawater such as temperature and salinity have significant effects on underwater flow noise levels [1]. The prediction of the underwater flow noise has been the target of those who have been researching in the field of acoustics for many years. However, flow noise around submerged bodies has not been well understood because of the complexity of the problem. Various noise sources emitted from different human activities vary significantly in terms of the frequencies and intensities (Table 1) [2,3,4,5].

Lu et al. calculated flow characteristics around the submarine and flow-induced noise using the FW-H method [9]. Svennberg and Fureby have also implemented a noise model, which can also be used for naval vessels, on a simpler geometry, as well as experimental work of the same model [10]. Moreau et al. conducted experimental studies on the flow noise around the wall-mounted cylinder with circular cross section and the square sectioned cylinder forms [11]. Choi et. al. performed noise analyses for a submerged cylinder using the FW-H method and the LES turbulence model without considering the quadrupole source terms [12]. Cianferra et al. analyzed three basic

geometries (sphere, cube, and spheroid) immersed in a uniform water stream to study on the differences in hydroacoustic areas [13]. Zhou estimated the flow noise caused by the air flow in a system where the cylinder and wing profile were used together [14]. Choi et al. (2017) examined the effect of quadrupole sources around a submerged circular cylinder. They proposed a hybrid model that reduces the computational cost of quadrupole sources [15].

Table 1. Various noise sources emitted from human activies in the sea [6, 7, 8]

Types of the Anthropogenic Sound	Frequency	Intensity Level
Pile driving	30–40 Hz	131–135 dB re 1 μPa
Drillship	20–1000 Hz	174–185 dB re 1 μPa
Navy Sonar	100–500 Hz	~215 dB re 1 μPa
Supertanker & container ship	6.8–70 Hz	180–205 dB re 1 μPa
Medium size ship (ferries)	~50 Hz	150–170 dB re 1 μPa
Boats (<30 m in length)	<300 Hz	~175 dB re 1 μPa
Small ship (support & supply ship)	20–1000 Hz	170–180 dB re 1 μPa

In the present work, the parameters affecting the flow noise around a circular cylinder have been investigated. The effects of parameters, such as temperature and salinity on acoustic spectrum at the harmonic frequencies have been examined. The flow-induced noise has been calculated numerically by solving Ffowcs Williams and Hawkings (FW-H) equations.

2. Theoretical Background

2.1. The Ffowcs Williams and Hawkings Method

The Ffowcs William and Hawkings method, based on the Lighthill analogy, allows prediction of a distant area loudness at some point. The nonlinear pressure fluctuations on the sound source surface are obtained by solving the flow equations. The obtained solution is integrated to calculate the pressure changes in the far field [16].

This method is based on Farassat's Formulation 1A of the FW-H analogy which uses an advanced-time formulation (or source time dominant algorithm) proposed by Casalino [17]. It yields the far-field acoustic pressure fluctuations computed using the FW-H formulations. FW-H equation includes monopole ($p'_T(\vec{x},t)$), dipole ($p'_L(\vec{x},t)$) and quadrupole ($p'_Q(\vec{x},t)$) sources (Eq. 1-4):

$$P'(\bar{x},t) = p_T'(\bar{x},t) + p_L'(\bar{x},t) + p_Q'(\bar{x},t) \tag{1}$$

$$p_T'(\bar{x},t) = \frac{1}{4\pi}\int_{(f=0)}\left[\frac{\rho_0(\dot{U}_n + U_{\dot{n}})}{r(1-M_r)^2} + \frac{\rho_0 U_n(r\dot{M}_r + a_0 M_r - a_0 M^2)}{r^2(1-M_r)^3}\right]_{ret} dS \tag{2}$$

$$p_L'(\vec{x},t) = \frac{1}{4\pi}\frac{1}{a_0}\int_{(f=0)}\left[\frac{\dot{\bar{L}}_r}{r(1-M_r)^2} + \frac{L_r(r\dot{\bar{M}}_r + a_0 M_r - a_0 M^2)}{r^2(1-M_r)^3}\right]_{ret} dS + \frac{1}{4\pi}\int_{(f=0)}\left[\frac{L_r - L_M}{r^2(1-M_r)^2}\right]_{ret} dS \quad (3)$$

where $L_i = P_{ij}\, n_i + \rho u_i(u_n - v_n)$ is load factor where $P_{ij} = (p - p_0)\delta_{ij}$. $U_i = \left[(\rho u_i)/\rho_0 + v_i(1-\rho/\rho_0)\right]$ and r represents the distance between source and observer, $r = x_{observer} - y_{face}$. u_i and v_i are, respectively, the fluid and surface velocity components in the x_i direction., and δ_{ij} corresponds to Kronecker delta. a_0 represents the speed of sound in the far-field area. ρ0 is the far-field reference density.

Farassat and Brentner [18] have shown that the noise contribution from the quadrupole, $(p_Q'(\vec{x},t))$, can be expressed as a "collapsing-sphere" formulation. Using this formulation, the space derivatives are transformed into time derivatives:

$$p_Q'(\vec{x},t) = \frac{1}{4\pi}\left(\left(\frac{1}{c}\right)\left(\frac{\partial^2}{\partial t^2}\right)\int_{-\infty}^{t}\left[\int_{(f>0)}\frac{T_{rr}}{r}d\Omega\right]d\tau + \left(\frac{\partial}{\partial t}\right)\int_{-\infty}^{t}\left[\int_{(f>0)}\frac{3T_{rr} - T_{ii}}{r^2}d\Omega\right]d\tau\right) + \left(c\int_{-\infty}^{t}\left[\int_{(f>0)}\frac{3T_{rr} - T_{ii}}{r^3}d\Omega\right]d\tau\right) \quad (4)$$

$\vec{M}$ is a local Mach number vector with components M_i, where $M_r = \vec{M}.\vec{r}$ and $L_M = L_i.M_i$. T_{ij} is the Lighthill stress tensor and $T_{rr} = T_{ij}r_i r_j$ describes the double contraction of T_{ij}.

Eqn. (4) is transformed from a collapsing-sphere formulation to an advanced time formulation using the following four equations. In these equations, the time derivatives at the observer are moved into the integrals to prevent numerical time differentiation of the integrals. The "source-time-dominant" algorithm from [19] is used to allow the estimation of the $(p_Q'(\vec{x},t))$, volume term of the FW-H equation as follows:

$$p_Q'(\vec{x},t) = \frac{1}{4\pi}\left(\int_{(f>0)}\left[\frac{K_1}{c^2 r} + \frac{K_2}{cr^2} + \frac{K_3}{r^3}\right]_{ret}\right) \quad (5)$$

$$K_1 = K_{11} + K_{12} + K_{13} = \left[\frac{\ddot{T}_{rr}}{(1-M_r)^3}\right] + \left[\frac{\ddot{M}_r T_{rr} + 3\dot{M}_{r\bar{T}}}{(1-M_r)^4}\right] + \left[\frac{3\dot{M}_r^2 T_{rr}}{(1-M_r)^5}\right] \quad (6)$$

$$K_2 = K_{21} + K_{22} + K_{23} + K_{24} = \left[\frac{-\ddot{T}_{rr}}{(1-M_r)^2}\right] + \left[\frac{4\dot{T}_{M_r} + 2T_{\dot{M}_r} + \dot{M}_r T_{ii}}{(1-M_r)^3}\right] + \left[\frac{3\left[(1-M^2)\dot{T}_{rr} - 2\dot{M}_r T_{Mr} - M_i \dot{M}_i T_{rr}\right]}{(1-M_r)^4}\right] + \left[\frac{6\dot{M}_r(1-M^2)T_{rr}}{(1-M_r)^5}\right] \quad (7)$$

$$K_3 = K_{31} + K_{32} + K_{33} = \left[\frac{2T_{MM} - (1-M^2)T_{ii}}{(1-M_r)^3}\right] + \left[\frac{6(1-M^2)T_{Mr}}{(1-M_r)^4}\right] + \left[\frac{3(1-M^2)^2 T_{rr}}{(1-M_r)^5}\right] \quad (8)$$

r_i denotes the unit vector in the direction of radiation. A dot above a variable denotes the time derivative with respect to source time of that variable.

2.2. Geometry and Modelling

The simulations have conducted considering three-dimensional (3D) computational domain, with a Reynolds number of $9x10^4$. The diameter of cylinder, D is 0.019 m and the cylinder length, L is 1.5 diameter of cylinder. The size of computational domain in y-direction is equal to 29.2D. The inlet and the outlet in the numerical simulations are placed respectively, 8.6D and 20.6D from the cylinder as shown in Figure 1. The computational domain at the top and bottom boundaries are both located at 10.3D from the cylinder axis.

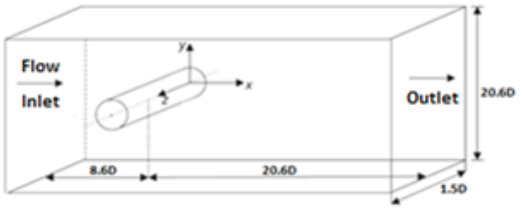

Figure 1. Physical configuration of the cylinder flow

A structured mesh is employed with 2894781 cells by locally refining the mesh in the near cylinder region and over the cylinder wake where the highest flow fluctuations are observed. A constant expansion of 1.2 is used in the radial direction away from the cylinder. A spatial mesh resolution of $\Delta y+ \approx 1$ is used on the cylinder wall to solve the near-wall flow. The smallest cell spacing in the radial direction is $r_{min}/D = 1.45 \times 10^{-4}$. In each layer along the length of the cylinder, 128 cells were placed along the circumference of the cylinder.

2.3. Computational Details

The acoustic calculations are performed for three temperature values (10 ^oC, 20 ^oC and 35 ^oC) and two salinity values (20 g/kg and 35 g/kg) for each temperature to investigate the effects of these parameters on the flow noise. It is also assumed that the fluid is incompressible and Newtonian. The physical properties of the fluid including density was changed by the fluid temperature. The receiver points for the acoustic analysis are placed perpendicular to the flow direction downward and respectively, 8 and 128 diameters away from the cylinder. The flow field results are used as the input data for the wave equations in order to attain the acoustic far-field. The acoustic and dynamic results are presented separately since the acoustic analogies are separated the flow field

and acoustic computations. The k–Omega SST (shear stress transport) model of Menter are used to simulate the flow past over the circular cylinder [20,21]. The numerical discretization scheme used to deal with the pressure-velocity coupling between the momentum and the continuity equations is the SIMPLE algorithm. The convection discretization is defined by using the segregated flow solver with second-order accuracy. The time discretization is performed by using an implicit and second-order accurate scheme. The Fast Fourier Transform (FFT) is used for the spectral analysis and Hann (Hanning) function is employed as the window function. The reference sound pressure is taken as 1 x 10^{-6} Pa for the acoustic analysis.

3. Results and Discussion

The numerical simulations are performed to investigate the effects of parameters, such as temperature and salinity, on the acoustic spectrum at the harmonic frequencies. The acoustic analysis is performed for a circular cylinder which was selected for the validation studies of the FW-H method [22]. Figure 2 shows the acoustic spectrum obtained from the validation studies by using k-ω SST turbulence model. They were compared with the corresponding experimental results of Revell et al. [23] and the numerical simulations of Orselli et. al. [24]. It is observed that FW-H method can predict discrete values of SPL associated with the fundamental frequency (Strouhal number) and the harmonic couples agrees well in timing.

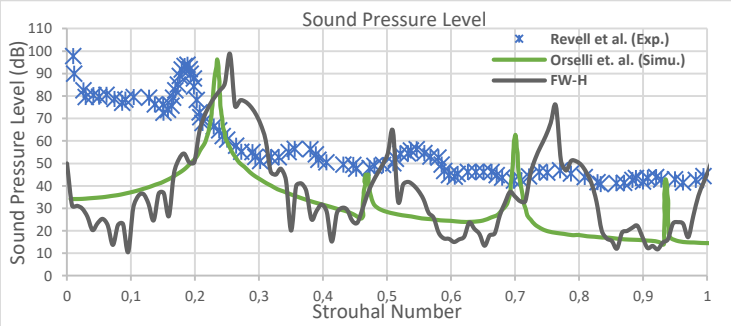

Figure 2. Sound Pressure Levels obtained from validation studies

Figure 3 and Figure 4 demonstrate the sound pressure levels obtained for various salinity and temperature values.

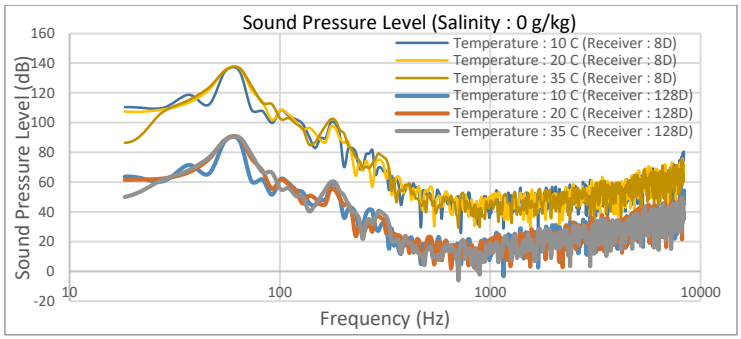

Figure 3. Sound Pressure Levels for various temperature values at the salinity of 0 g/kg

The sound pressure levels are presented depending on the frequency spectrum. For the receiver point A1 at 8 diameters away from the cylinder, the broadband noise is between 40 dB and 80 dB, while this value is between 20 dB and 50 dB for receiver point A2 at 128 diameters away from cylinder. It is seen that there is a decrease about 40 % (25 dB) in the broadband noise, when the distance between the receiver and cylinder is increased by 16 times. The peak frequency, which the maximum sound pressure level occurs, is approximately 64 Hz.

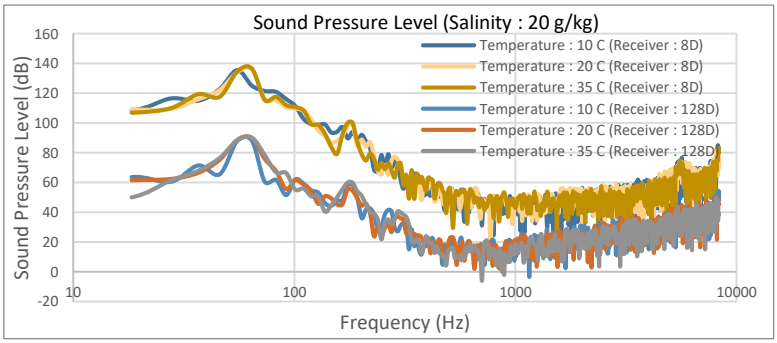

Figure 4. Sound Pressure Levels for various temperature values at the salinity of 20 g/kg

Figure 5 and Figure 6 present the variation of the maximum sound pressure levels according to different salinity and temperature values for two different receiver points (A1 and A2). As can be observed from these figures that the maximum sound pressure level increases as the temperature increases for both salinity values (0 g/kg and 20 g/kg).

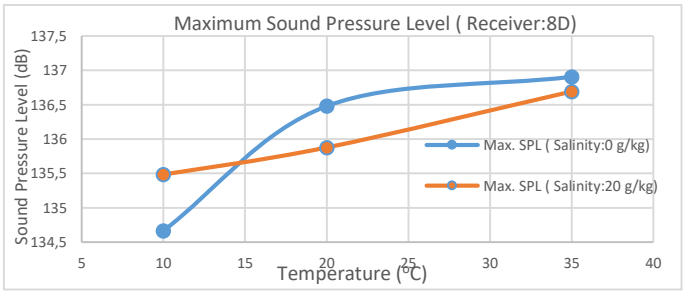

Figure 5. Maximum Sound Pressure Levels for the receiver point A1

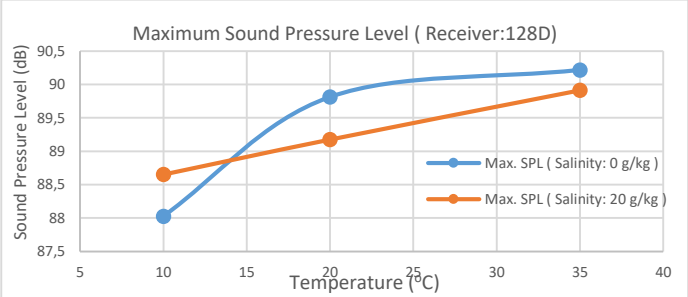

Figure 6. Maximum Sound Pressure Levels for the receiver point A2

The increase in the salinity at the temperature, 10°C leads to a decrease in the sound pressure level, while at higher temperature values above about 15ºC, the sound pressure level decreases with increasing salinity value. It is also observed that there is a decrease about 35% (47 dB) in the broadband noise, when the distance between the receiver and the cylinder is increased by 16 times.

Figure 7 and Figure 8 show the overall sound pressure levels (OASPL) for each acoustic spectrum for two different receiver points. It is observed that the OASPL increases with increasing temperature, but decreases with increasing salinity. The magnitude of the decrease is greater, especially at the temperature of 10ºC. There is a decrease about 35% (45 dB) in the broadband noise, when the distance between receiver and cylinder is increased by 16 times.

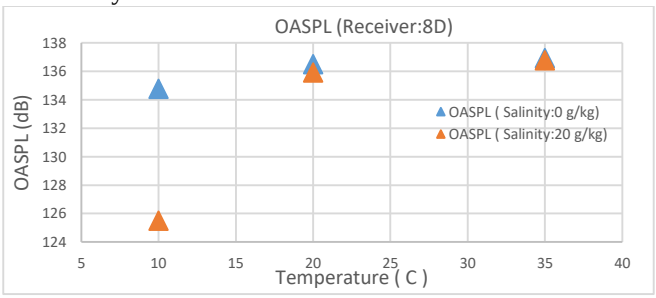

Figure 7. Overall Sound Pressure Levels for the receiver point A1

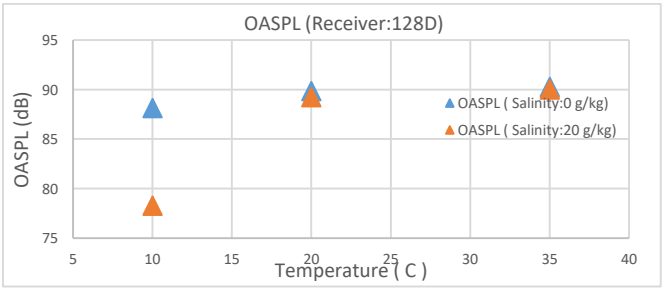

Figure 8. Overall Sound Pressure Levels for the receiver point A2

4. Conclusions

The investigation of the effects of temperature and salinity on the flow noise around a circular cylinder has been performed by using FW-H method. The sound pressure levels are obtained at various receiver positions for three temperature values and two salinity values. It is found that there is a decrease about 40 % (25 dB) in broadband noise, when the distance between receiver and cylinder is increased by 16 times. There is a direct correlation between the temperature and both maximum SPL and OASPL. The increase in salinity at 10°C leads to a decrease in the sound pressure level, while at the temperatures above about 15ºC, the sound pressure levels increase. The OASPL increases with increasing temperature, but decreases with increasing salinity.

References

[1] C. Peng, X. Zhao, G. Liu, Noise in the Sea and Its Impacts, Int. J. Environ. Res. Public Health **12** (2008), 12304-12323.

[2] R. K. Andrew, B. M. Howe, J. A. Mercer, Ocean ambient sound: Comparing the 1960s with the 1990s for a receiver off the California coast, Acoustics Research Letters Online **3** (2002), 65.

[3] A. Slotte, K. Hansen, J. Dalen, E. Ona, Acoustic mapping of pelagic fish distribution and abundance in relation to a seismic shooting area off the Norwegian west coast, Fisheries Research **67** (2004), 143-150.

[4] M. A. McDonald, J. A. Hildebrand, S. M. Wiggings, Increases in deep ocean ambient noise in the Northeast Pacific west of San Nicolas Island, California, *Acoustical Society America* **120-2** (2006), 711-8.

[5] D. Ross, Ship sources of ambient noise, IEEE Journal of Oceanic Engineering 30 (2005),257–261.

[6] W. J. Richardson, K. J. Finley, G. W. Miller, R. A. Davis, W. R. Koski, Feeding, social and migration behavior of bowhead whales, Balaena mysticetus, in Baffin Bay vs. the Beaufort Sea—Regions with different amount of human activity, Marine Mammal Science **11** (1995), 1-45.

[7] Conservation and Development Problem Solving Team. Anthropogenic Noise in the Marine Environment: Potential Impacts on the Marine Resources and Stellwagen Bank and Channel Islands National Marine Sanctuaries; University of Maryland: Maryland, MD, USA, 2000;pp. 18–19.

[8] Gisiner, R.; Cudahy, E.; Frisk, G.; Gentry, R.; Hofman, R.; Popper, A.; Richardson, W.J. Proceedings: Workshop on the Effects of Anthropogenic Noise in the Marine Environment; Office of Naval Research (1998), 141.

[9] L. Yun-tao, Z. Huai-xin, P. Xu-jie, Numerical simulation of flow-field and flow-noise of a fully appendage submarine, Journal of Vibration and Shock, Shanghai Jiao Tong University 2008

[10] U. Svennberg, C. Fureby, Vortex-Shedding Induced Trailing-Edge Acoustics, Swedish Defence Research Agency, Stochholm 2010.

[11] D. J. Moreau, C. Doolan, Flow-induced Sound of Wall-Mounted Finite Length Cylinders, AIAA Journal **51** (2013), 10.

[12] W. Choi, Y. Choi, S. Hong, J. Song, H. Kwon, C. Jung, Turbulence-induced Noise of a Sub-merged Cylinder Using a Permeable FW-H Method,*Int. Journal of Naval Arc. and Ocean Eng.* **8**(2016), 235-242.

[13] M. Cianferra, V. Armenio, S. Ianniello, Hydroacoustic noise from different geometries, International Journal of Heat and Fluid Flow (2017).

[14] B. Y. Zhoi, T. Albring, N. R. Gauger, Evaluation of Different Methods in Computational Aeroacoustics for Noise Prediction and Minimization of a Rod-Airfoil Configuration, 24th International Congress on Sound Vibration, London, 2017.

[15] Y. Choi, W. Choi, S. Hong, J. Song, H. Kwon, H. Seol, C. Jung, Development of formulation Q1As method for quadrupole noise prediction around a submerged cylinder, International Journal of Naval Architecture and Ocean Engineering **9** (2017), 484-491.

[16] J. E. Williams, D. L. Hawkings, Sound Generation by Turbulence and Surfaces in Arbitrary Motion. *Philosophical Transactions of the Royal Society of London* **264** (1969), 321-342.

[17] D. Casalino, M. Jacob, Prediction of Aerodynamic Sound from Circular Rods via Spanwise Statiscal Modelling, *J. Sound and Vibration* **262** (2003), 815-844.

[18] K.S. Brentner, F. Farassat, Analytical Comparison of the Acoustic Analogy and Kirchoff Formulation for Moving Surfaces, *AIAA Journal* **36-8** (1998), 1379-1386.

[19] D. Casalino, An advanced time approach for acoustic analogy predictions, *J Sound and Vibration* **261-4**(2003), 583-612.

[20] F. R. Menter,Zonal Two Equation k-ω Turbulence Models for Aerodynamic Flows,*AIAA*(1993),93-2906.
[21] F. R. Menter, Two-Equation Eddy-Viscosity Turbulence Models for Engineering Applications, *AIAA* **32-8** (1994), 1598-1605.
[22] S.Ergin, S.Bulut, Estimating Flow-Induced Noise of a Circular Cylinder Using Numerical and Analytical Acoustic Methods, IMAM 2017, Lisbon, 2017.
[23] R. M. Orselli, J. R. Meneghini, F. Saltara, Two and Three-Dimensional Simulation of Sound Generated by Flow around a Circular Cylinder, 15th AIAA/CEAS Aeroacoustics, Miami, Florida, 2009.
[24] J.D. Revell, R. A. Prydz, A. P. Hays, Experimental Study of Airframe Noise vs. Drag Relationship for Circular Cylinders, *Lockheed Report 28074, Final Report for NASA Contract NAS1-14403*,1997.